

Re-evaluation of the low-energy Coulomb-dissociation cross section of ${}^8\text{B}$ and the astrophysical S_{17} factor

K. Sümmerer^a

For the S223 Collaboration^b
GSI Darmstadt, Germany

Received: 22 July 2005 /

Published online: 10 March 2006 – © Società Italiana di Fisica / Springer-Verlag 2006

Abstract. An exclusive measurement of the Coulomb breakup of ${}^8\text{B}$ into ${}^7\text{Be}+p$ at 254 A MeV was used to infer the low-energy ${}^7\text{Be}(p, \gamma){}^8\text{B}$ cross section. Particular emphasis was placed on the angular correlations of the breakup particles which demonstrate clearly that $E1$ multipolarity dominates within the angular cuts selected for the analysis. The deduced astrophysical S_{17} factors exhibit good agreement with the most recent direct ${}^7\text{Be}(p, \gamma){}^8\text{B}$ measurements.

PACS. 25.40.Lw Radiative capture – 25.60.-t Reactions induced by unstable nuclei – 25.70.De Coulomb excitation – 26.65.+t Solar neutrinos

1 Introduction

The flux measured in neutral-current interactions of high-energy solar neutrinos by the Sudbury Neutrino Observatory (SNO) [1, 2] is in general agreement with the flux predicted by the standard solar model (SSM, refs. [3, 4]). It is essential, however, to further reduce the uncertainty of nuclear inputs to the SSM in order to refine its predictions. One critical quantity is the ${}^7\text{Be}(p, \gamma){}^8\text{B}$ cross section at solar energies since it is linearly related with the high-energy solar neutrino flux stemming from ${}^8\text{B}$ β -decay.

In recent years, many attempts have been undertaken to measure this cross section (or, equivalent, the astrophysical S_{17} factor) with high-precision in direct-proton-capture measurements using radioactive ${}^7\text{Be}$ targets [5, 6, 7, 8]. A completely different approach with different systematic errors is Coulomb dissociation (CD) of ${}^8\text{B}$ in the electromagnetic field of a high- Z nucleus. Such measurements have been performed at intermediate [9, 10] and

high energies [11]. This contribution reports on a CD experiment similar to that of ref. [11], but with an improved experimental technique. Preliminary results of this study have been published earlier [12]. In the present contribution we present a re-evaluation of the published data and show that the efficiency to detect low-energy break-up events was slightly overestimated. As a consequence, the lowest data points are increased by about 6–10% which suggests a different theoretical model to extrapolate to zero energy than used in ref. [12]. We have recently published a full account of the present work [13].

2 Theoretical calculations

Realistic theoretical calculations of the CD of ${}^8\text{B}$ are essential for several reasons. From a practical point of view, the relatively bad energy resolution of the CD method requires to simulate, *e.g.*, the effect of cross talk between neighboring energy bins, of the finite size and resolution of the tracking detectors etc. These simulations require a CD event generator that is reasonably close to reality so that the remaining differences between the measured and simulated cross-section distributions can be attributed to the S_{17} factor. As input to the event generator we have to specify a nuclear model for ${}^8\text{B}$ and choose a method to calculate Coulomb dissociation.

The simplest model for ${}^8\text{B}$ is that of a p -wave proton coupled to an inert ${}^7\text{Be}$ core with $I^\pi = 3/2^-$ to form the ${}^8\text{B}$ ground state with $I^\pi = 2^+$. With this model we obtain astrophysical S -factors as a function of the proton- ${}^7\text{Be}$ relative energy, E_{rel} , as shown in fig. 1. The non-resonant

^a e-mail: k.suemmerer@gsi.de

^b Members of the S223 Collaboration are F. Schümann and F. Strieder (Universität Bochum); S. Typel, K. Sümmerer, F. Uhlig, H. Geissel, P. Koczon, N. Kurz, E. Schwab, P. Senger, and Zhi-Yu Sun (GSI Darmstadt); F. Hammache (IPN Orsay); D. Cortina (Universidad Santiago de Compostela); A. Förster, H. Oeschler, and C. Sturm (TU Darmstadt); I. Boettcher, B. Kohlmeyer and M. Menzel (Universität Marburg); M. Gai (University of Connecticut); U. Greife (Colorado School of Mines); N. Iwasa (Tohoku University); R. Kulesa, M. Ploskon, W. Prokopowicz, G. Surowka, and W. Walus (Krakow University); H. Kumagai, T. Motobayashi, and A. Ozawa (RIKEN); A. Wagner and E. Grosse (FZ Rossendorf).

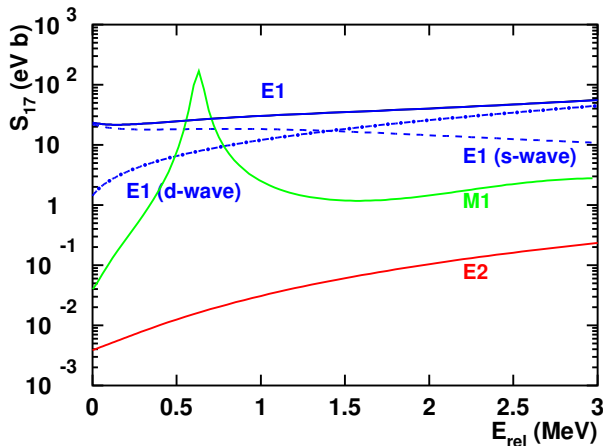


Fig. 1. Theoretical S_{17} factors from a simple potential model of ${}^8\text{B}$ and their decomposition into contributions from various partial waves.

direct capture into the ${}^8\text{B}$ ground state proceeds mainly via s - and d -wave captures and $E1$ γ -emission. Capture of p - and f -waves followed by $E2$ emission plays an insignificant role, in particular at solar energies. The resonant component proceeds through the 1^+ resonance at 633 keV above threshold which decays mainly by $M1$ emission and is limited essentially to a narrow region around the resonance energy.

Coulomb dissociation of ${}^8\text{B}$ on ${}^{208}\text{Pb}$ at 254 A MeV is calculated in the semi-classical model in first-order perturbation theory (PT), as described in more detail elsewhere [14, 15, 16]. This approach should be a good approximation at the high bombarding energy used. Due to the large number of $E2$ photons present in the virtual photon spectrum seen by the ${}^8\text{B}$ projectile, one can assume the $E2$ component to be significantly enhanced compared to the direct-capture case. This will be investigated experimentally in our experiment.

3 Experimental procedures

The ${}^8\text{B}$ secondary beam was produced at the SIS/FRS radioactive beam facility at GSI [17] by fragmenting a 350 A MeV ${}^{12}\text{C}$ beam in a 8 g/cm^2 Be target and separating it from contaminant ions in a 1.4 g/cm^2 wedge-shaped Al degrader placed in the FRS intermediate focal plane. Typical ${}^8\text{B}$ beam intensities in front of KaoS were 5×10^4 ions per 4 s spill; the only contaminant consisted of about 20% ${}^7\text{Be}$ ions which could be identified event by event with the help of a time-of-flight measurement. For this purpose a 3 mm thick plastic scintillator detector was installed in the transfer line between FRS and KaoS, about 85 m upstream from the breakup target, to serve as a time-of-flight (ToF) start detector. Positions and angles of the secondary beam incident on the Pb breakup target were measured with the help of two parallel-plate avalanche counters (PPAC) located at 308.5 cm and 71 cm upstream from the target, respectively. The detectors had areas of

$10 \times 10\text{ cm}^2$ and allowed to track the incident ${}^8\text{B}$ beam with about 99% efficiency and with position and angular resolutions of 1.3 mm and 1 mrad, respectively. In addition, they provided a ToF stop signal with a resolution of 1.2 ns (FWHM). The ${}^8\text{B}$ energy at the target was 254 A MeV and was limited by the maximum bending power of the KaoS spectrometer.

A schematic view of the experimental setup used in the present experiment to detect the breakup of ${}^8\text{B}$ in semi-complete kinematics at the KaoS spectrometer at GSI is shown in fig. 2. Apart from the PPAC tracking detectors mentioned above, it consisted of i) the ${}^{208}\text{Pb}$ break up target; ii) two pairs of Si strip detectors; iii) the magnets of the KaoS spectrometer; iv) two large-area multi-wire proportional chambers (MWPC); v) a ToF wall serving as a trigger detector.

Downstream from the Pb target (52 mg/cm^2 of ${}^{208}\text{Pb}$), the angles and positions as well as the energy losses of the outgoing particles were measured with two pairs of single-sided Si strip detectors (SSD, $300\ \mu\text{m}$ thick, $100\ \mu\text{m}$ pitch) located at distances of about 14 cm and 31 cm downstream from the target.

The KaoS magnetic spectrometer [18] consisted of a large-aperture quadrupole and a horizontally focussing dipole magnet. To avoid multiple scattering of the fragments in air, the chamber inside the quadrupole and dipole magnets was filled with He gas at 1 bar pressure.

Behind the magnets, two large-area MWPC were installed as close to the focal plane as possible. One chamber, with horizontal and vertical dimensions of 60 cm and 40 cm, respectively, detected the position of protons behind KaoS. The other one, 120 cm wide and 60 cm high, was set to detect the ${}^8\text{B}$ non-interacting beam and the ${}^7\text{Be}$ fragments.

Behind the focal plane and parallel to it, a plastic-scintillator wall with 30 elements (each 7 cm wide and 2 cm thick) was installed and used for trigger purposes. The wall was subdivided into two sections. Coincident signals in the left-hand (proton) part and in the right-hand (ion) part of the wall indicated a break-up event (“breakup” trigger). Singles hits in the right hand section were interpreted as “beam” triggers and recorded with a down-scale factor of 1000.

4 Data reduction and results

The experiment described in the present paper recorded events from three different sources:

- i) break-up events originating in the Pb target;
- ii) down-scaled beam particles;
- iii) background from a variety of sources (*e.g.*, cosmic rays).

Though event classes i) and ii) are mainly correlated with a corresponding trigger type (“breakup” trigger for class i), “beam” trigger for class ii)) we have checked if by chance the trigger types and event classes were mixed in rare cases, and have corrected for that.

The coincident p and ${}^7\text{Be}$ signals resulting from breakup in the ${}^{208}\text{Pb}$ target were identified among the

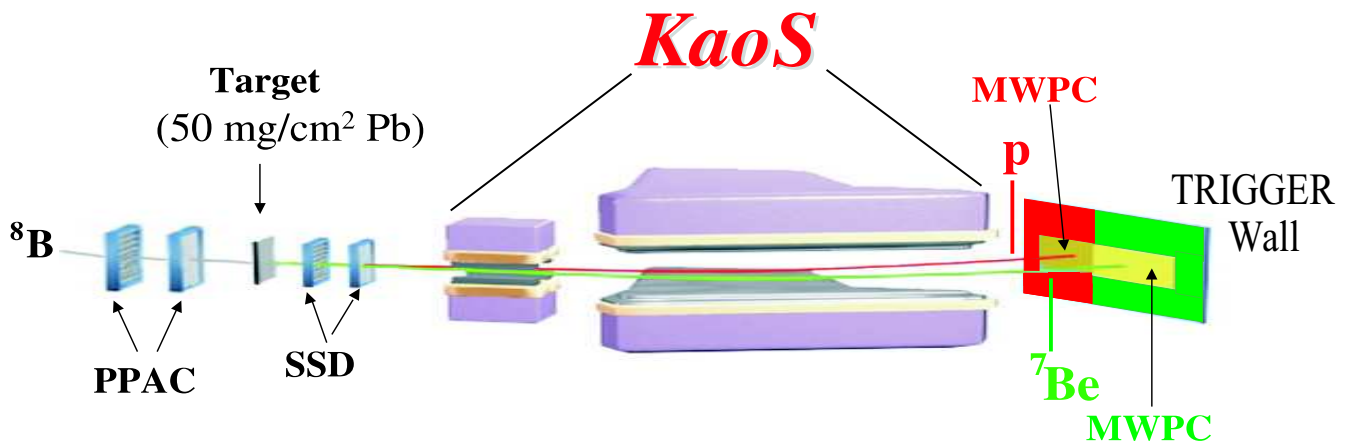


Fig. 2. Artist's view of the experimental setup. Shown schematically are the beam-tracking detectors (PPAC) in front of and the fragment-tracking Si strip detectors (SSD) behind the Coulomb-breakup target. Proton and ^7Be positions in the focal plane of the KaoS magnetic spectrometer are determined by large-area multi-wire chambers (MWPC) followed by a scintillator-paddle wall for trigger purposes.

class i) events (“breakup” trigger) in several successive steps:

- 1) The ΔE -ToF condition was applied to select only incident ^8B ions (see above).
- 2) A multiplicity of $m \geq 2$ in each SSD was required. This required that at least one empty strip was found between two respective hit clusters.
- 3) A 3σ -window around the ΔE peak corresponding to the energy loss of ^7Be in each SSD selected those events where ^8B was converted into ^7Be .
- 4) The coincident protons were found among all events with $\Delta E < 500$ keV in each SSD the trajectories of which converged towards the target. Moreover, their closest distance to the ^7Be trajectory was required to lie inside a volume given in x and y by the size of the target (± 18 mm in x - and ± 12 mm in y -direction) and having a z -value along the beam axis of ± 25 mm around the target (located at $z = 0$).

The inclusive ΔE spectra resulting from conditions 1 and 2 above are shown by the thin intermediate line in fig. 3, whereas conditions 3 and 4 lead to the full innermost histograms in fig. 3. This procedure removed all breakup events in layers of matter other than the target and led to a practically background-free measurement.

4.1 Invariant-mass reconstruction

The p- ^7Be relative energy, E_{rel} , is derived from the total energies, E_i , of the particles i ($i = \text{p}, \text{Be}$), their 3-momenta, p_i , and the p-Be opening angle, θ_{17} , according to

$$E_{rel} = \sqrt{(E_{\text{Be}} + E_{\text{p}})^2 - p_{\text{Be}}^2 - p_{\text{p}}^2 - 2p_{\text{Be}}p_{\text{p}} \cos(\theta_{17})}. \quad (1)$$

To reconstruct a breakup event, the p and ^7Be hits in each SSD have to be separated by at least one empty strip.

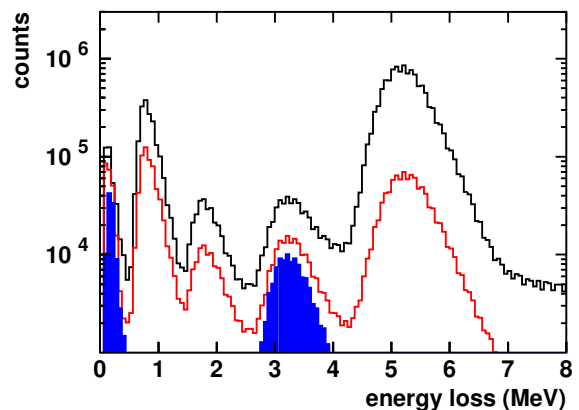


Fig. 3. Energy-deposition of the incident ^8B ions and of the break-up fragments in the third Si strip detector. The outermost contour corresponds to all events. The thin intermediate contour depicts events where an incident ^8B particle is correlated with multiplicity $m = 2$ in each SSD. The full innermost histograms are obtained by requiring a ΔE -cut on ^7Be in each SSD plus a p- ^7Be vertex inside the target volume (see text).

Since this affects the efficiency for identifying a breakup event for low E_{rel} , we have to make sure that the GEANT simulation accurately reproduces this efficiency. This has been achieved by introducing a weighting function in GEANT that gradually increases the efficiency for detecting two separated hits from zero to one over the appropriate distance for each detector so that experimental and simulated distance distributions look alike. In fig. 4 we plot the inclusive horizontal distances between proton and ^7Be hits in the first SSD. One can observe that experiment and simulation yield very similar distributions. It should be emphasized that in our earlier data analysis a step function of this efficiency was assumed that jumped from zero to full efficiency at a fixed distance of 0.4 mm in each SSD. This is visualized by the dashed histogram in

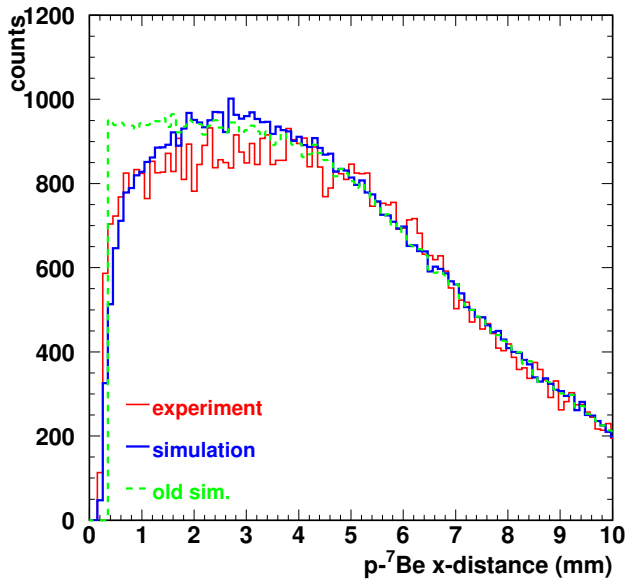


Fig. 4. Horizontal (x -) distances between proton and ${}^7\text{Be}$ hits in the first Si strip detector. The thin line shows the distribution of experimental distances, the thick one results from the present GEANT simulation. The dashed histogram shows the GEANT simulation that was used to evaluate our previous results [12].

fig. 4; it clearly shows that we overestimated the GEANT detection efficiency for small p - ${}^7\text{Be}$ distances (small E_{rel}) in our previous paper [12].

4.2 Angular distributions

In the following we will present some angular distributions that can be shown to be sensitive to an $E2$ amplitude in CD. With ${}^8\text{B}^*$ we denote the reference system of the (excited) ${}^8\text{B}$ prior to breakup. Its momentum vector is reconstructed from the measured proton and ${}^7\text{Be}$ momentum vectors. The angle θ_8 is the laboratory scattering angle of ${}^8\text{B}^*$ relative to the incoming ${}^8\text{B}$ beam. The polar angles, θ_{cm} , and the azimuthal angles, ϕ_{cm} , of the break-up protons are measured in the rest frame of the ${}^8\text{B}^*$ system. In the same way, one can calculate the transverse proton momentum vector in the reaction plane (p_t^{in}).

Figure 5 shows the θ_8 distribution, in comparison to two-model calculations using first-order PT. The full histogram denoting pure $E1$ multipolarity follows the data points very well, even to very large angles. The dashed histogram, where both $E1$ and $E2$ with their full theoretical strength were assumed, deviates from the data points markedly for θ_8 values above about 0.7 degrees. Note that the theoretical histograms were folded with the experimental response. We conclude that this distribution already indicates $E1$ dominance.

We present in fig. 6 the distribution of p_t^{in} for three different upper limits in θ_8 , 0.6° , 1.0° , and 2.5° . In classical Rutherford scattering, this corresponds to impact

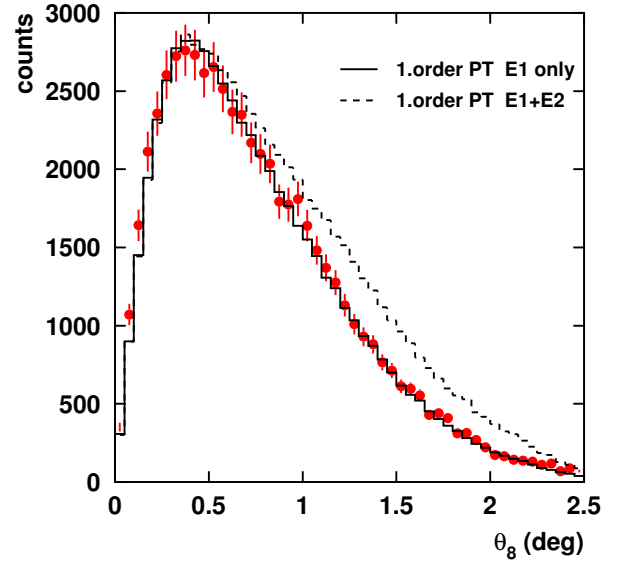


Fig. 5. Scattering angle θ_8 of the excited ${}^8\text{B}$ prior to breakup, as reconstructed from the proton and ${}^7\text{Be}$ vectors. The full histogram has been calculated in first-order perturbation theory assuming pure $E1$ multipolarity, the dashed one assuming $E1+E2$ multipolarity.

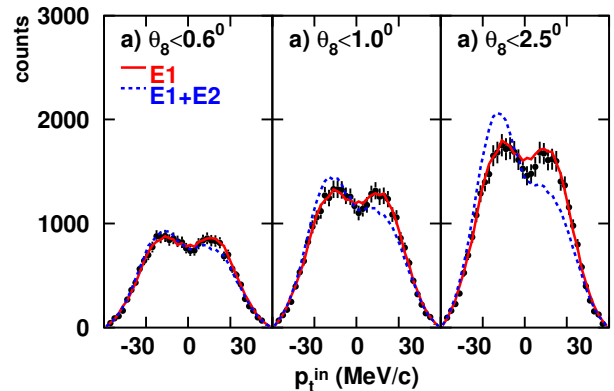


Fig. 6. In-plane transverse momenta, p_t^{in} , of the breakup protons for three different cuts in θ_8 . The theoretical curves (full lines: $E1$ multipolarity, dashed lines: $E1+E2$ multipolarity) have been calculated in first-order perturbation theory. They were normalized individually to the data points in each frame.

parameters of 30 fm, 19 fm, and 7 fm, respectively. Relative energies between p and ${}^7\text{Be}$ up to 1.5 MeV were selected. The experimental data for all three θ_8 -cuts can be reproduced well by a PT calculation that includes only $E1$ multipolarity (full histograms in fig. 6, the theoretical curves were normalized individually to the data points). If $E1$ -plus- $E2$ multipolarity is used in the PT calculation, the different impact-parameter dependences of $E1$ and $E2$ multipolarity lead to markedly different shapes for the different θ_8 -cuts (dashed histograms in fig. 6). In particular for large values of θ_8 , the latter distributions show a strong anisotropy around $p_t^{in} = 0$ which is absent in our data. This is a very sensitive test of $E2$ admixture and again shows no substantial $E2$ contribution.

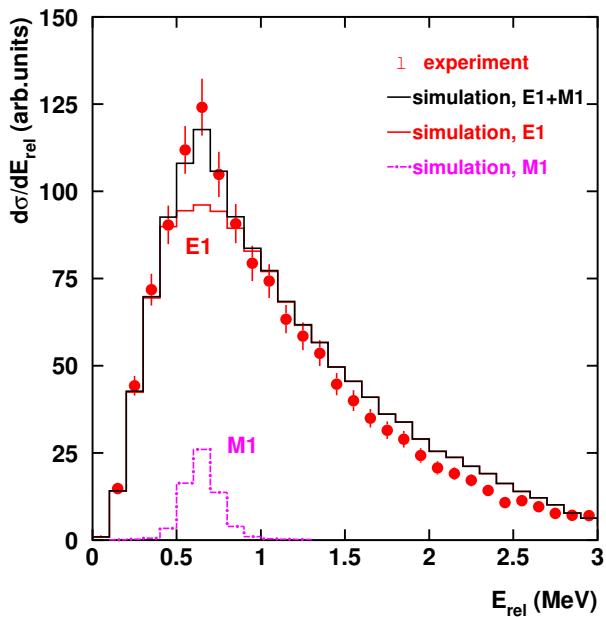


Fig. 7. Energy-differential Coulomb-dissociation yields for equal-sized E_{rel} bins of 100 keV each. The thick outermost histogram results from our GEANT simulation including $E1$ and $M1$ multipolarity, scaled by a factor of 0.82. The thin (dot-dashed) histograms show the separate contributions from $E1(M1)$ multipolarity.

4.3 Energy-differential dissociation yields

The measured momentum vectors of the outgoing p and ${}^7\text{Be}$ particles allowed to calculate E_{rel} according to eq. (1), from which we have constructed the energy-differential dissociation yields of the excited ${}^8\text{B}^*$ system prior to breakup (fig. 7). In line with our findings of a negligible $E2$ contribution discussed above, we compare this spectrum to a simulated one that contains contributions from $E1$ and $M1$ multiplicities only. The latter contribution was calculated using the $M1$ resonance parameters as determined by Filippone *et al.* [19].

In plotting fig. 7, we have restricted the Rutherford scattering angles θ_8 to values below 1.0° to ensure both dominance of CD and reduction of the effect of any possible $E2$ contribution. After determining an absolute $E1$ normalization factor of $f = 0.82$, the experimental and simulated distributions agree rather well. Small deviations between the data points and the black histogram indicate discrepancies between the assumed S_{17} factor from our potential model and the true one, as will be discussed in the next section.

5 The astrophysical S_{17} factor

The measured quantity in CD of ${}^8\text{B}$ is the distribution of energy-differential cross sections, fig. 7. This distribution is related to S_{17} via a theoretical model. We assume that at the high incident energy used in our experiment

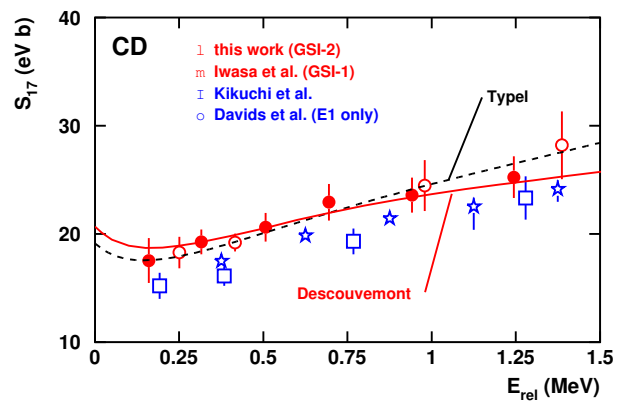


Fig. 8. Comparison between S_{17} values from Coulomb-dissociation experiments. The full (open) circles indicate the present (previous) GSI CD experiment labelled GSI-2 (GSI-1). Open stars depict ref. [9], open squares ref. [10] ($E2$ contribution subtracted). The theoretical curves are described in the text.

and for the low Q -value of the reaction, first-order perturbation theory is adequate to describe Coulomb dissociation. In analyzing our results, we also assume that the GEANT simulations describe all experimental effects quantitatively, in particular the feeding of neighboring bins due to the relatively bad E_{rel} resolution. Any remaining discrepancies between the two histograms in fig. 7 are attributed to a deviation of the true $E1$ S_{17} factor from the one used in our simulation. Thus, the true S_{17} factor for each bin was obtained by multiplying the theoretical one (averaged over the bin width) by the ratio of observed and simulated counts. The resulting S_{17} factors as a function of E_{rel} are visualized in fig. 8.

5.1 Comparison with other CD experiments

Figure 8 shows our astrophysical S_{17} factors in comparison with those from the other three CD experiments published so far [9, 11, 10] (the data of ref. [10] represent their $E1$ - S_{17} factors after subtraction of the $E2$ contribution). The CD S_{17} factors are in reasonable agreement, though both the Kikuchi *et al.* [9] and the Davids *et al.* [10] data are systematically lower. We note also that our earlier CD experiment [11] and the present one are in good agreement in this energy range, marked discrepancies occur only at higher E_{rel} values. Compared to the results given in ref. [12], the lowest three data points have been modified to become larger by 6.7%, 10%, and 5.8%, respectively, due to a smaller efficiency to detect two separate break-up products in the SSD, as explained in subsect. 4.1 and visualized in fig. 4. The remaining data points remain largely unaffected. As a consequence, the slope of our S_{17} factors as a function of E_{rel} becomes smaller and fits much better than previously to the energy dependence of Descouvemont's cluster model [20, 21].

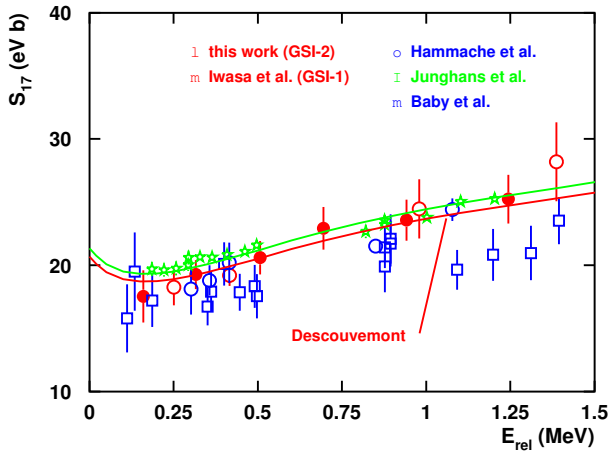


Fig. 9. S_{17} from this work in comparison with the (p, γ) experiments of ref. [5] (squares), ref. [8] (stars), and ref. [7] (open circles). The latter data were corrected for the contribution of the $M1$ resonance by the authors. The theoretical curves are from Descouvemont [21] and have been fitted to the Seattle data (upper curve) and the present data (lower curve), respectively. See text for more details.

5.2 Comparison with direct-capture experiments

Figure 9 compares our data to those of the recent ${}^7\text{Be}(p, \gamma){}^8\text{B}$ measurements where the authors have subtracted the contribution from the $M1$ resonance (refs. [5, 7, 8]). With the modifications of the lowest- E_{rel} data points discussed above, our dataset follows now closely the (p, γ) data of Junghans *et al.* [8] over their *entire* energy range.

5.3 Extrapolation to zero relative energy

To extrapolate to zero energy, we have chosen the recent cluster-model calculation of Descouvemont [21] (we refer to this model below as D04). In this refined approach, the curve resulting from the Minnesota force (MN) is closer to the experimental data and has been used in fig. 9 to fit both the Seattle data and our present results over the energy range up to $E_{rel} = 1.5$ MeV. The fits yield practically identical results within their respective errors.

Our previous data set [12] was found to be best compatible with the potential-model calculation of Typel as discussed in subsect. 2 of the present paper or in Davids and Typel [14] (referred to below as DT03). It is obvious that with the modified low-energy data points of the present paper, the agreement with this model is less satisfactory. The black dashed curve in fig. 8 visualizes a fit of this theory to our data.

When we fit our lowest 8 data points, up to $E_{rel} = 2$ MeV, to the D04 model, we obtain $S_{17}(0) = 20.6 \pm 0.8$ eV b. A systematic error of 5.6% has to be added, yielding $S_{17}(0) = 20.6 \pm 0.8(stat) \pm 1.2(syst)$ eV b. Not included in these numbers is the theoretical uncertainty

given by Descouvemont [21] as about 5–10% depending on the relative energy.

6 Conclusions

We conclude that at sufficiently high incident energy, a high-resolution exclusive CD experiment can provide a rather precise value for the low-energy ${}^7\text{Be}(p, \gamma){}^8\text{B}$ cross section. By setting tight constraints to the scattering angle, θ_8 , and analyzing proton- ${}^7\text{Be}$ angular correlations, a significant contribution from $E2$ multipolarity could be excluded. Contrary to our earlier publication [12], our re-analyzed results for the astrophysical S_{17} factor follow closely the energy dependence as predicted by the refined cluster-model description of Descouvemont [21]. This finding is in line with the most recent measurements of the ${}^7\text{Be}(p, \gamma){}^8\text{B}$ reaction. The combined statistical and systematic errors of our fit value for $S_{17}(0)$ amounts to 6.6%; a similar error contribution of about 5% comes from the model uncertainty [21].

The authors wish to thank K.-H. Behr, K. Burkard, and A. Brünle for technical assistance. Vivid discussions with B. Davids, P. Descouvemont, M. Hass, and A. Junghans are gratefully acknowledged.

References

1. Q.R. Ahmad *et al.*, Phys. Rev. Lett. **89**, 011301; 011302 (2002).
2. SNO Collaboration, arXiv:nucl-ex/0502021.
3. J.N. Bahcall, M.H. Pinsonneault, Phys. Rev. Lett. **92**, 121301 (2004).
4. S. Turck-Chieze *et al.*, Phys. Rev. Lett. **93**, 211102 (2004).
5. F. Hammache *et al.*, Phys. Rev. Lett. **86**, 3985 (2001).
6. F. Strieder *et al.*, Nucl. Phys. A **696**, 219 (2001).
7. L.T. Baby *et al.*, Phys. Rev. Lett. **90**, 022501 (2003).
8. A.R. Junghans *et al.*, Phys. Rev. C **68**, 065803 (2003).
9. T. Kikuchi *et al.*, Phys. Lett. B **391**, 261 (1997); T. Kikuchi *et al.*, Eur. Phys. J. A **3**, 213 (1998).
10. B. Davids *et al.*, Phys. Rev. C **63**, 065806 (2001).
11. N. Iwasa *et al.*, Phys. Rev. Lett. **83**, 2910 (1999).
12. F. Schümann *et al.*, Phys. Rev. Lett. **90**, 232501 (2003).
13. F. Schümann *et al.*, Phys. Rev. C **73**, 015806 (2006).
14. B. Davids, S. Typel, Phys. Rev. **68**, 845802 (2003).
15. C.A. Bertulani, Phys. Rev. C **49**, 2688 (1994); Z. Phys. A **356**, 293 (1996).
16. S. Typel *et al.*, Nucl. Phys. A **613**, 147 (1997), implemented as code CDXS by S. Typel (2002).
17. H. Geissel *et al.*, Nucl. Instrum. Methods Phys. Res. B **70**, 286 (1992).
18. P. Senger *et al.*, Nucl. Instrum. Methods Phys. Res. B **327**, 393 (1993).
19. B.W. Filippone *et al.*, Phys. Rev. C **28**, 2222 (1983).
20. P. Descouvemont *et al.*, Nucl. Phys. A **567**, 341 (1994).
21. P. Descouvemont, Phys. Rev. C **70**, 065802 (2004).